Applied Catalysis B: Environmental 256 (2019) 117774

Contents lists available at ScienceDirect

Applied Catalysis B: Environmental

journal homepage: www.elsevier.com/locate/apcatb

In-situ electrode fabrication from polyaniline derived N-doped carbon nanofibers for metal-free electro-Fenton degradation of organic contaminants

Muhammad Rizwan Haider[a,b], Wen-Li Jiang[a,b], Jing-Long Han[a,b], Hafiz Muhammad Adeel Sharif[a,b], Yang-Cheng Ding[a,b], Hao-Yi Cheng[a,b], Ai-Jie Wang[a,b,*]

[a] Key Laboratory of Environmental Biotechnology, Research Center for Eco-Environmental Sciences, Chinese Academy of Sciences, Beijing, 100085, PR China
[b] University of Chinese Academy of Sciences, Beijing, 100049, PR China

ARTICLE INFO

Keywords:
Electro-fenton
Metal-free
Polyaniline derived carbon catalyst
Binder-free electrode

ABSTRACT

Electro-Fenton (e-Fenton) process is a highly efficient technology for refractory wastewater treatment. However, electrode fabrication from powdered carbon catalysts usually requires additional binders, which is expensive, non-scalable and arduous process. In this study, the electrode was in-situ fabricated using N-doped carbon nanofibers derived from carbonization of polyaniline (PANI), electrodeposited on graphite-felt substrate without any binder. The as synthesized electrode was used for in-situ electro-generation and activation of H_2O_2 to $^{\bullet}OH$ radicals for degradation of organic pollutants without metal catalyst. Potassium hydroxide was used to tailor the functional groups and reactive surface area of the electrode. The optimized electrode showed H_2O_2 production of 0.306 mg cm^{-2} h^{-1} and 85% of phenol removal with 42% of mineralization in 180 min. Mainly the N functional groups (graphitic and pyridinic N) function as active sites for electro-generation and activation of H_2O_2 to $^{\bullet}OH$ radicals, which was the main oxidant for degradation of pollutants.

1. Introduction

Electrochemical advanced oxidation processes (EAOPs), based on strong and non-selective oxidants, are widely studied techniques for the degradation of refractory organic pollutants in recent years due to the high mineralization efficiency, environmental friendliness and widespread applications [1,2]. As one of the EAOPs, electro-Fenton (e-Fenton) process is considered to be a promising technology, where H_2O_2 is in situ generated from the two-electron oxygen reduction reaction (2e– ORR) at the cathode (Eq. (1)), which reacts with the metal catalyst to produce $^{\bullet}OH$ (Eq. (2)) [3,4].

$$O_2 + 2H^+ + 2e^- \rightarrow H_2O_2 \quad (1)$$

$$H_2O_2 + Fe^{2+} + H^+ \rightarrow Fe^{3+} + {}^{\bullet}O\,H + H_2O \quad (2)$$

The H_2O_2 production is mainly governed by the type and characteristics of the cathode material [5]. Currently, carbon-based materials as e-Fenton cathode are gaining much attention by the researchers due to their favorable H_2O_2 generation, low-cost, non-toxic, good stability and high conductivity [4]. Accordingly, many different types of carbonaceous materials like carbon/graphite felt [6,7], carbon nanotubes [8], carbon black/PTFE [1] and graphene [9,10] have been investigated for enhanced production of H_2O_2 and its application in degradation of refractory organic pollutants in wastewater. The activation of H_2O_2 to $^{\bullet}OH$ is crucial for e-Fenton process and usually achieved with dissolved ferrous salts as iron catalyst. However, separation and disposal of iron residue that cause secondary pollution is a major challenge [11]. Although, significant efforts have been made to overcome this issue by developing efficient heterogeneous Fenton-like catalysts [12,13], it is hard to completely overcome the metal leaching problem [14,15]. Therefore, metal-free catalyst would be an interesting choice to activate H_2O_2 to $^{\bullet}OH$.

Recently, it has been reported that carbonaceous materials can efficiently catalyze $^{\bullet}OH$ production from in situ generated H_2O_2 without any additional metal catalyst for refractory wastewater treatment [16,17]. It eliminates the need for metal catalyst and overcomes an intrinsic drawback of secondary pollution, which would ultimately reduce the treatment cost. To address the catalytic ability of metal-free carbocatalysts, Yang et al. developed nitrogen doped graphene modified electrode, which enhanced the in situ generation of H_2O_2 and its

* Corresponding author at: Key Laboratory of Environmental Biotechnology, Research Center for Eco-Environmental Sciences, Chinese Academy of Sciences, Beijing, 100085, PR China.
E-mail address: ajwang@rcees.ac.cn (A.-J. Wang).

https://doi.org/10.1016/j.apcatb.2019.117774
Received 18 April 2019; Received in revised form 22 May 2019; Accepted 23 May 2019
Available online 05 June 2019
0926-3373/

activation to ˙OH that resulted in higher degradation efficiency as compared to non-nitrogen doped graphene as well as the traditional e-Fenton [18,19]. In a recent study, they found the pyridinic nitrogen as an active site for the conversion of H_2O_2 to ˙OH [20]. These interesting pioneering works inspired us to explore new possibilities to develop metal-free e-Fenton cathodes.

Though considerable improvements have been made in e-Fenton cathode materials, mostly catalysts are discretely produced in powder form. Electrode fabrication from the powder materials is a complicated and expensive process [11,21], and usually prepared by coating catalyst layer on a solid support using some polymer binders (Supporting Information (SI) Fig. S1). However, non-conductive binders such as PTFE could decrease the electrode capacitance and conductivity [22], block access to the active sites (Fig. S1) [7] and reduce the permeability of ions at the electrode-electrolyte interface [23]. In addition, adhesion between the catalyst and solid support becomes weaker in long-term operation, and possible release of catalyst or binder could result in secondary pollution. Besides, this commonly adopted approach for electrode fabrication is difficult to scale up [11].

Recently, polyaniline (PANI) has been widely studied as nitrogen containing carbon precursor due to low cost, high nitrogen content and easy synthesis [24–26]. Especially, electro-polymerization of aniline is a facile synthesis route for direct coating of PANI on a conducting substrate without any binders [27,28]. In addition, the graphite like structure of PANI could facilitate introduction of the different nitrogen moieties (as pyridinic, pyrrolic and graphitic nitrogen) into the carbon framework during high temperature pyrolysis [29]. As reported, pyridinic nitrogen is the active site in carbon framework for in situ electro-generation [30] and activation of H_2O_2 to ˙OH [20]. The PANI derived carbons have been successfully applied as adsorbents [31], electrocatalysts [32] and supercapacitors [24]. However, according to the best of author's knowledge, no report has been conducted so far about PANI derived carbon used as metal-free catalyst in e-Fenton system.

Herein we report novel e-Fenton cathode, in situ fabricated from PANI derived N-doped carbon nanofibers for electro-generation and activation of H_2O_2 to ˙OH without metal catalyst. The modified cathode was synthesized by electrochemical polymerization and carbonization of PANI on a graphite felt (GF) substrate without using any binder. Potassium hydroxide (KOH) was used as a green activating agent for tuning the surface properties of the cathode. The effects of different KOH ratios on surface functional groups and its influence on electro-generation of H_2O_2 and degradation performance of organic contaminants were investigated using phenol as a pollutant. The phenol degradation performance of the as prepared cathode was also compared with the metal-based e-Fenton system. Besides overcoming the metal leaching problem, this novel cathode synthesis process is facile, binder-free and without any toxic chemicals, which makes it scalable, cost-effective, safe and environmentally friendly.

2. Experimental

2.1. Binder-free electrode fabrication

The metal-free e-Fenton electrode was in situ fabricated by direct polymerization and carbonization of PANI on GF according to the process schematically illustrated in Fig. 1. As depicted, firstly, PANI was electro deposited on GF substrate through a facile and green electrochemical synthesis route. In a typical modified procedure adopted from elsewhere [24–26], pre-wet GF (2.5 × 3 cm^2) was first immersed in 100 mL of 0.1 M aniline aqueous solution (0.5 M H_2SO_4) and sonicated for 5 min for homogeneous wetting of the substrate with the electrolyte. Cyclic voltammetry (CV) within a potential range of –0.2 to 1.2 V (scan rate 10 mV s^{-1}) for 5 cycles was used for electro-polymerization of aniline monomer in a three-electrode electrochemical cell with GF, stainless steel mesh (2.5 × 3 cm^2) and Ag/AgCl as a working, counter and reference electrodes, respectively. After polymerization process, PANI nanofibers coated GF (PANI/GF) was carefully washed with deionized (DI) water and dried at 60 °C overnight.

The PANI derived N-doped carbon nanofibers modified electrode was then obtained in a two-step carbonization and activation process. First, the as prepared PANI/GF was carbonized in a quartz furnace at 500 °C for 2 h under N_2 protection to obtain cPANI/GF. Then a certain amount of KOH (KOH to cPANI ratio of 1, 2 and 4, where cPANI weight was obtained by subtracting initial GF weight from total weight after first carbonization) as a green activating agent was dissolved in a minimum amount of Milli-Q water and the as obtained cPANI/GF was immersed and shaken for 1 h for thorough and homogeneous wetting of the electrode. Then, the water was evaporated at 85 °C and KOH covered cPANI/GF was obtained, which was activated at 700 °C for 1 h under N_2 protection. After cooling down to room temperature, the obtained cPANI/GF1, cPANI/GF2 and cPANI/GF4 were thoroughly washed with 2 M HCl and DI water (until stable pH) and dried under vacuum prior to use. The final loading amount of coated material for cPANI/GF1, cPANI/GF2 and cPANI/GF4 was 3.95 mg cm^{-2}, 3.39 mg cm^{-2}, and 3.09 mg cm^{-2}, respectively.

2.2. Characterization

Morphology of the as prepared electrode was observed with a field emission scanning electron microscope (FESEM, model SU-8020, Hitachi, Japan) and a transmission electron microscope (TEM, Tecnai G2 F30, FEI). Surface elemental composition was studied by X-ray photoelectron spectroscopy (XPS) using ESCLAB 250 Xi spectrometer (Thermo Fisher Scientific). Fourier transform infrared spectrometer (FTIR, TENSOR 27, Bruker, Germany) was also used to confirm successful deposition and subsequent carbonization of PANI nanofibers. The Brunauer-Emmett-Teller (BET) specific surface area was determined with micromeritics (ASAP 2460 USA), Surface Area Analyser using the N_2 adsorption-desorption isotherm data.

For electrochemical characterizations, CV and linear sweep voltammetry (LSV) analysis were performed by electrochemical workstation (CHI 660e) in a three-electrode electrochemical cell using Na_2SO_4 (0.05 M) aqueous solution as electrolyte saturated with either O_2 or N_2. The as synthesized electrode was used as a working electrode with dimensionally stable anode (DSA) and Ag/AgCl as counter and reference electrode, respectively.

2.3. Metal-free e-Fenton degradation experiment

Experiments for refractory organic contaminants degradation with the metal-free e-Fenton cathode were conducted in an undivided three-electrode electrochemical cell containing 100 mL of 0.05 M Na_2SO_4 solution (pH 3.0) as electrolyte with 50 mg/L of phenol, florfenicol (FLO) or methyl orange (MO) as a pollutant. In a potential controlled electrolysis (CHI 660e), the as synthesized electrode was used as a working electrode (cathode) with DSA (2.5 × 3 cm^2) and Ag/AgCl as a counter and reference electrodes, respectively. The electrolyte was continuously supplied with compressed air at a constant flow rate of 0.6 L/min.

The concentration of H_2O_2 was measured by spectrophotometric method at maximum absorbance wavelength of 402 nm [33]. The hydroxyl free radicals were detected with electron spin resonance (ESR) spectroscopy by using 5,5-dimethyl-1-pyrroline N-oxide (DMPO) as a trapping agent [34]. The concentration of phenol was analysed by HPLC (DGU 20A3R, Shimadzu, Japan) equipped with a photodiode array (PDA) detector using a C18 column (5 µm; 150 × 4.6 mm, Waters Ldt. Co., USA) at a maximum wavelength of 270 nm. The mobile phase was methanol and water (80:20, v: v) with a flow rate of 1 mL/min [35]. The same equipment was used to analyse the FLO concentration with methanol and water (55:45, v: v) as mobile phase at a flow rate of 0.8 mL/min [36]. The MO concentration of was measured using spectrophotometer at maximum wavelength of 467 nm. Total organic

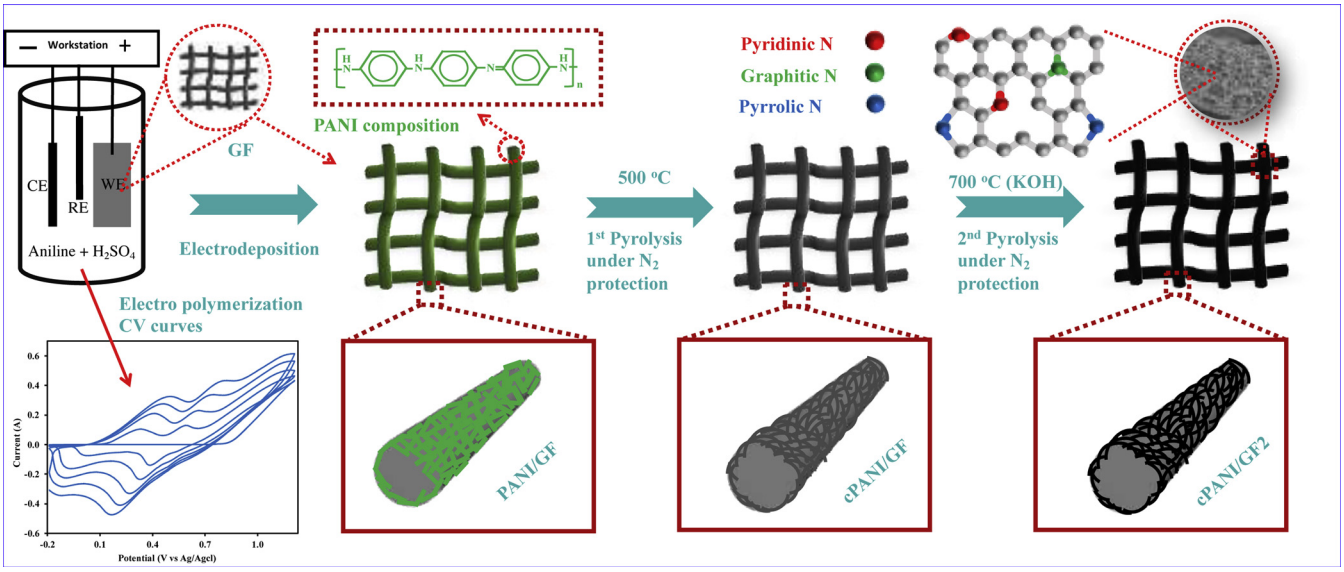

Fig. 1. Schematic illustration of the binder-free in situ fabrication of PANI derived carbon nanofibers modified electrode.

carbon (TOC) was measured by TOC analyser (TOC-L CPH, Shimadzu, Japan).

3. Results and discussion

3.1. Characterization of the modified electrode

Surface morphologies of the GF, PANI/GF and cPANI/GF2 are presented in Fig. 2. The GF fiber initially has a smooth surface (Fig. 2a), which was uniformly covered by PANI (Fig. 2b) after electro polymerization of aniline monomer confirming the formation of PANI/GF composite. The PANI nanorods with a diameter of 105–170 nm evolved into an interconnected, cross-linked macro porous conducting network of nanofibers. The cPANI/GF2, obtained after carbonization and activation step, perfectly retained the morphology of cross-linked nanofibers (Fig. 2c–d) even after high temperature pyrolysis with KOH [24]. The macro pores in cPANI/GF2 were widened (Fig. 2d), mainly due to reduction in diameter of nanofibers to about 78–104 nm by strong KOH etching. Cross-linking between highly conducting nanofibers could reduce the internal resistance and improve electron transfer, while widened macro pores increased the accessible active surface area.

Microstructure of the cPANI/GF2 was also examined by TEM and the results are presented in Fig. 2e–f. The cross-linked macro porous network of nanofibers could be seen clearly (Fig. 2e), which remained unchanged even after scratching from GF substrate and long time ultrasonication during sample preparation for TEM analysis. It indicate a strong covalent bond between nanofibers [26], which formed an interconnected network around the GF fibers resulting in a stable cPANI/GF2 composite without additional binders. The high-resolution TEM (HR-TEM) analysis revealed the coexistence of amorphous and graphitized carbon, with 3–4 graphitic layers mainly at the edges (Fig. 2f), which is in consistence with the reported literature [37,38]. The lower degree of graphitization might be due to the lower temperature used for activation (700 °C for 1 h). Partially graphitized carbon may facilitate the introduction of nitrogen containing active sites during heat treatment [29]. Moreover, chemical composition of the cPANI/GF2 was analyzed by elemental mapping, which showed C, N and O as main elements with the uniform distribution (Fig. 2g–i).

Surface chemistry of the electrode significantly affects its catalytic performance, which was tuned by KOH activation in this study. Therefore, XPS analysis was conducted to gain insights into the surface chemistry of the electrode, which changes obviously during fabrication process and the results are shown in Fig. 3. Two peaks, including C1s and O1s were shown in the survey spectra for GF (Fig. 3a). Another distinct N1s peak appeared in the survey spectra for PANI/GF obtained after PANI polymerization over GF substrate, which was also found in that of cPANI/GF2 obtained by pyrolysis, revealing that the electrode was doped with nitrogen successfully. Similar findings were also revealed by the FTIR spectra for GF, PANI/GF and cPANI/GF2 (Fig. S2a). The high-resolution N1s spectra of PANI/GF (Fig. 3b) revealed four typical peaks appeared at 398.67 eV (–N=), 399.8 eV (–NH–), 400.4 eV ($–NH^+=$) and 401.85 eV ($–NH_2^+–$), confirming the successful synthesis of PANI over GF substrate [39,40]. After pyrolysis, one main peak at 284.65 eV (C=C) corresponding to graphitic sp2 C atoms [41] appeared in the C1s spectra of cPANI/GF2 (Fig. 3c), implying successful carbonization of PANI/GF composite. It occupied about 70% of the total peak area and reportedly facilitates the 2e– ORR process for H_2O_2 production [20,42]. In addition, two more peaks appeared at 285.6 and 286.85 eV could be assigned to C—N and C—OH [39], which showed successful incorporation of N and O functional groups into the carbon matrix. Furthermore, the N1s spectra of cPANI/GF2 could be deconvoluted into four characteristics peaks appeared at 398.6, 400.4, 401.5 and 402.5 eV attributable to pyridinic N, pyrrolic N, graphitic N and pyridinic N oxides, respectively [24,43]. As mentioned earlier, graphitic N and pyridinic N are considered to be the active sites for H_2O_2 production and its activation to $^{\bullet}OH$ [20].

The surface elemental composition and their content (atomic %) calculated from XPS peak area is presented in Table 1. The content of C, O and N changed obviously with concentration of KOH, indicating that the carbon matrix was restructured during activation process. Particularly the content of nitrogen was drastically reduced from 3.78 to 1.08 at.% when the KOH ratio increased from 1 to 4 (wt./wt.), which was in accordance with the reported literature where similar trends were observed for nitrogen reduction [24,44,45]. The authors explained that N groups were probably eliminated from carbon matrix by KOH at elevated temperature. Similarly, the content of pyridinic N and pyrrolic N was also reduced, but for graphitic N, it increased first with KOH ratio increasing from 1 to 2 and then decreased when KOH ratio was further increased to 4. This could be ascribed to the conversion of pyridinic N and pyrrolic N to graphitic N by ring opening and condensation process under sever pyrolysis conditions [46]. The KOH activation also introduced micro pores, which increased the specific surface area as shown in Fig. S2b that would facilitate the mass transfer of reactants to the active sites for enhanced reaction.

For electrochemical characterization of the electrode, CV and LSV analysis were performed and the results are presented in Fig. 4. The

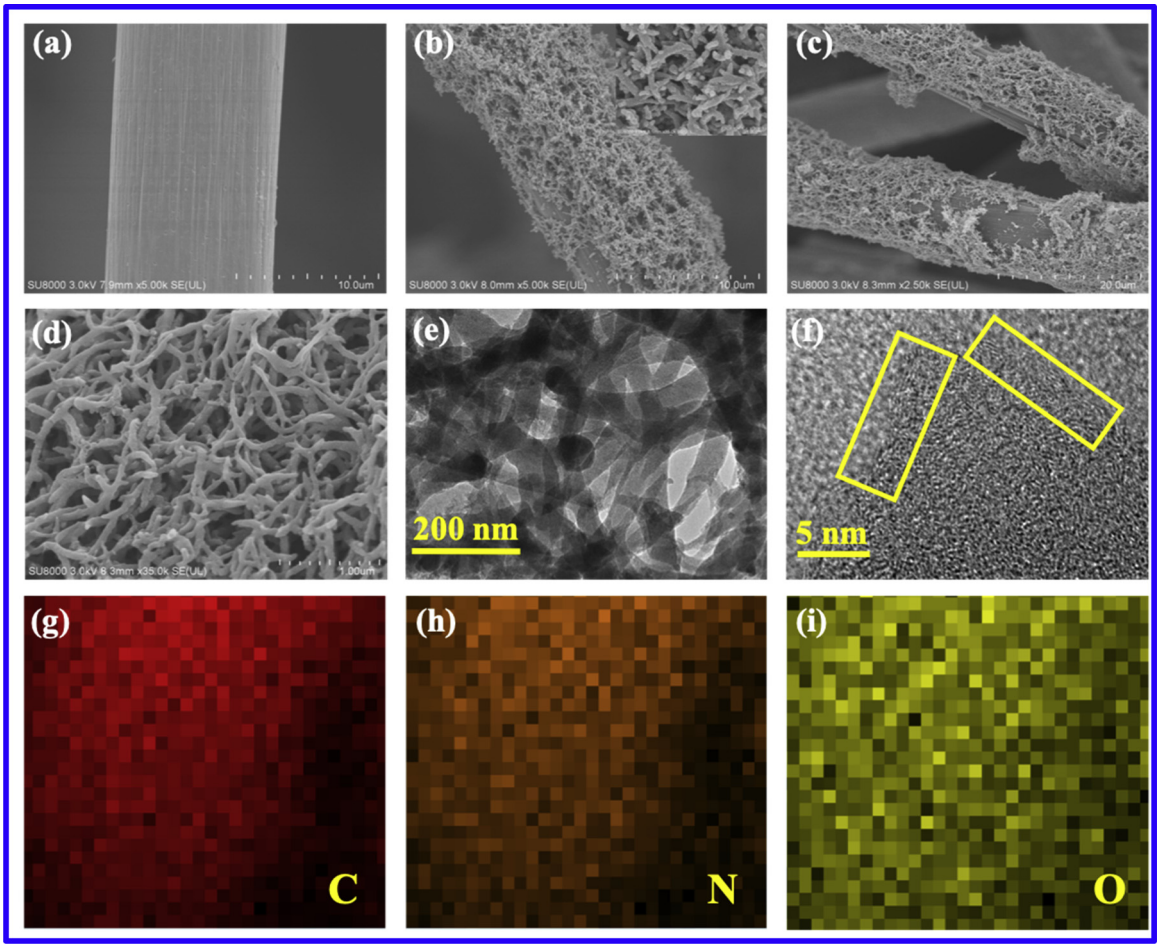

Fig. 2. SEM images of GF (a), PANI/GF (b), cPANI/GF2 (c–d); TEM (e), HRTEM (f) and elemental mapping (g–i) of cPANI/GF2.

reduction current for cPANI/GF2 was obviously higher for the O_2 saturated electrolyte as compared to the N_2 saturated (Fig. 4a), which was due to the reduction of oxygen at the cathode surface [19]. The LSV analysis also showed comparatively higher current response in the O_2 saturated conditions (Fig. 4b), further revealing that oxygen could be efficiently reduced on the modified cPANI/GF2 electrode. The current response for unmodified GF electrode in the O_2 saturated conditions was lower than cPANI/GF2 for both O_2 and N_2 saturated conditions. It might be due to decrease in charge transfer resistance or increase in electro-active surface area of the electrode after modification, which increased the rate of electrochemical reactions [9,22]. Charge transfer resistance and electro-active surface area of the cPANI/GF2 was studied by electrochemical impedance spectroscopy (EIS) and redox reactions of Fe^{III}/Fe^{II} by cyclic voltammetry. A relatively depressed semicircle by cPANI/GF2 in the high frequency region of the impedance spectra (Fig. S4a) suggested a decrease in the charge transfer resistance as compared to GF, which is in accordance with the literature [26]. Furthermore, the peak current of cPANI/GF2 was 6.9 times higher than that of GF in the CV curve of Fe^{III}/Fe^{II} redox couple (Fig. S4b), which showed a significant increase in the electro-active surface area [9,10,47]. This improvement could be attributed to the interconnected, cross-linked conducting network of nanofibers without any binders [26].

3.2. Degradation of pollutants with the modified electrode

The as synthesized metal-free cPANI/GFx was directly used as cathode in the e-Fenton system for phenol degradation and the results are shown in Fig. 5. The cPANI/GF2 showed the highest performance for phenol degradation, H_2O_2 production and TOC removal efficiency, while cPANI/GF1 showed the lowest. The catalytic performance of the cPANI/GF1 increased with the KOH ratio increasing from 1.0 to 2.0 and then decreased with the ratio further increasing to 4.0. It was interesting to note that while the specific surface area increased from cPANI/GF1 to cPANI/GF4 (Fig. S2b), the nitrogen content decreased, reaching an equilibrium at cPANI/GF2. This phenomenon suggested a trade-off between specific surface area and nitrogen content for enhanced catalytic performance of the cathode. Furthermore, carbonization might have created some defects [26], which could promote oxygen chemisorption and improve its electrochemical reduction [7,42], however, carbon material may collapse under sever pyrolysis conditions [7,48] resulting in decreased catalytic performance by the cPANI/GF4 cathode. The KOH was used as a green activating agent to tailor the surface properties of the electrode instead of very high temperature pyrolysis [49,50] that could reduce the heating cost during the synthesis process. Thus, the nitrogen content and specific surface area could be easily tuned by simply adjusting the amount KOH.

The better performance of cPANI/GF2 can also be attributed to its balanced doping of N content and bonding configurations, which is essential for optimum performance of the catalyst [26]. Relatively higher content of C=C (70.5 at.%), high oxygen content (4.34 at.%) and graphitic N (0.29 at.%) (Fig. S3 and Table 1) would result in a higher H_2O_2 production [4,20,42] (Fig. 5b), which could be further activated by the pyridinic N to produce high amount of $^{\bullet}OH$ for superior degradation and mineralization of phenol. Although the nitrogen content of cPANI/GF1 was higher than that of cPANI/GF2 and cPANI/GF4, its H_2O_2 production and phenol degradation efficiency was lower, which might be due to relatively low surface area and less reactive sites available for oxygen diffusion and reaction. In addition, the content of

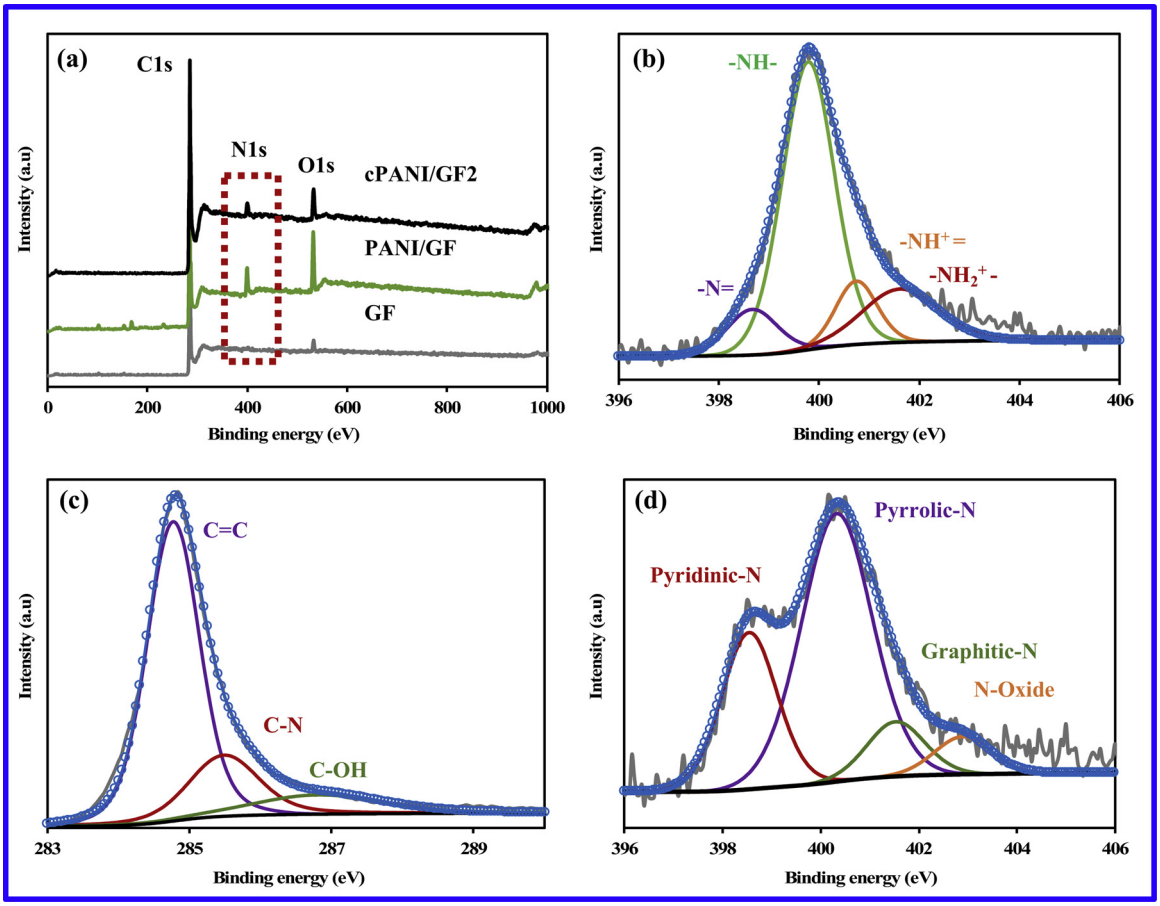

Fig. 3. XPS survey spectra (a), the high-resolution N1s spectra of PANI/GF (b), and C1s (c) and N1s (d) spectra of cPANI/GF2.

Table 1
Surface elemental composition (atomic %) of modified electrode.

Sample	C	O	N	N1s		
				Pyridinic N	Pyrrolic N	Graphitic N
PANI/GF	72.68	23.11	4.21	–	–	–
cPANI/GF1	91.90	4.32	3.78	1.17	2.39	0.22
cPANI/GF2	92.87	4.34	2.79	0.80	1.70	0.29
cPANI/GF4	95.90	3.02	1.08	0.31	0.64	0.13

pyrrolic N (2.39 at.%) was relatively high, which is reportedly the active site for 4e– ORR [51], shifting the reaction towards conversion of O_2 to H_2O (Eq. (3)). Furthermore, the pyridinic N in cPANI/GF2 (0.8 at. %) was more close to the content already reported in literature [18–20] for best catalytic performance. In summary, the higher specific surface area along with the high graphitic N content would provide more reactive sites that could enhance the H_2O_2 production, whereas at the same time, the high pyridinic N could activate the produced H_2O_2 to higher amount of $^{\cdot}OH$ for enhanced degradation of the pollutants.

$$O_2 + 4H^+ + 4e^- \rightarrow 2H_2O \quad (3)$$

The degradation of organic pollutants during e-Fenton process is

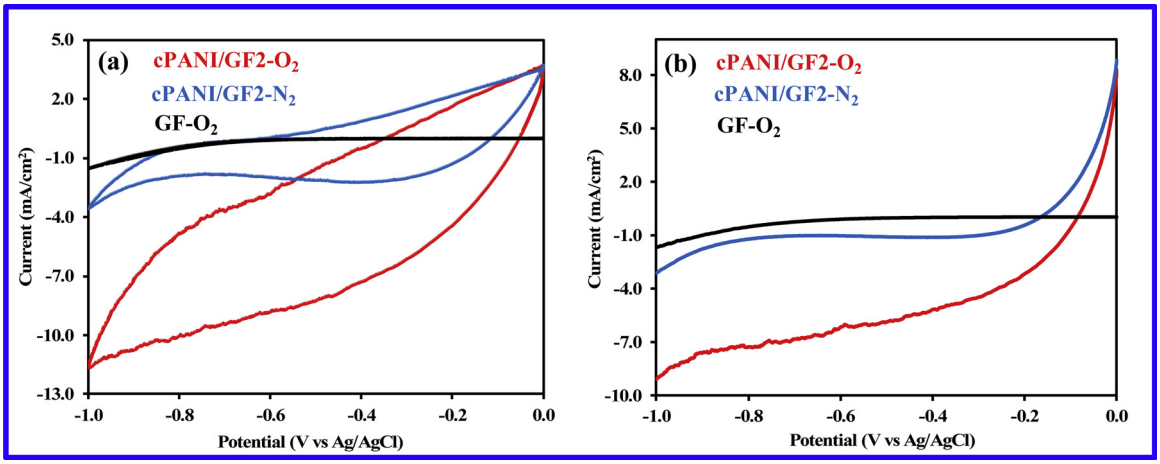

Fig. 4. Cyclic voltammetry (a) and linear sweep voltammetry curves (b) of GF and cPANI/GF2 in O_2/N_2 saturated Na_2SO_4 solution.

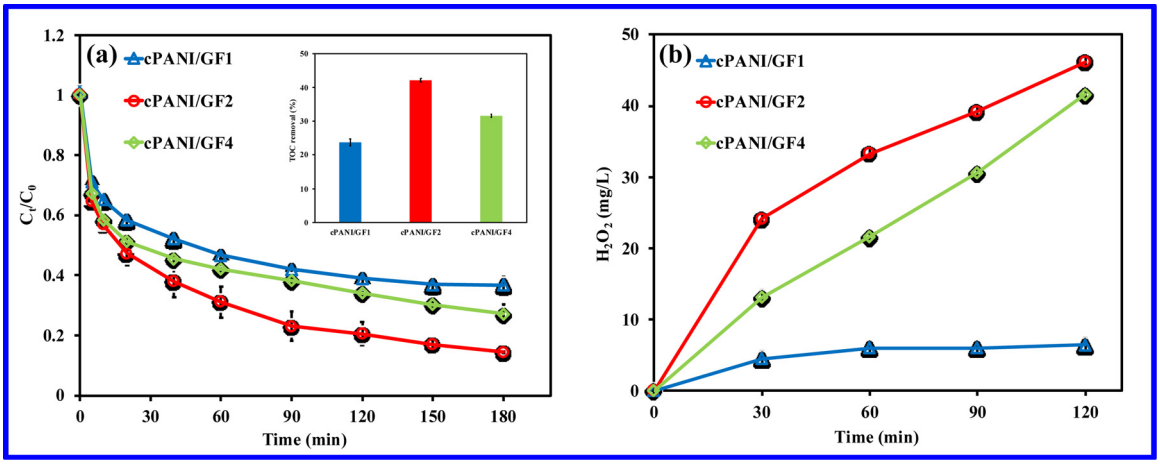

Fig. 5. Metal-free e-Fenton degradation of phenol (a) and H_2O_2 production efficiency (b) of cPANI/GF activated at different KOH ratios. Inset is the TOC removal efficiency. Conditions: V 100 mL, 0.05 M Na_2SO_4 at pH 3, C_0 50 mg/L, potential -0.6 V v Ag/AgCl.

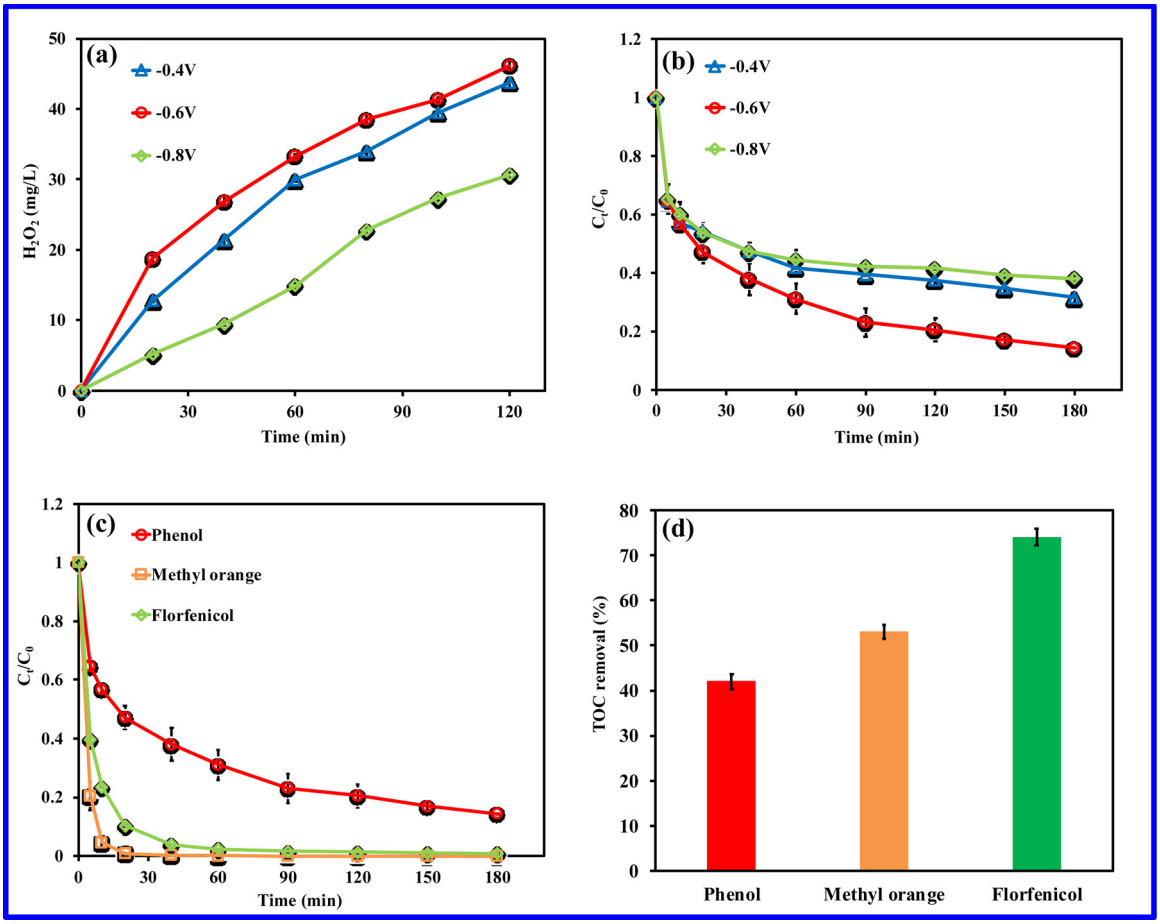

Fig. 6. The influence of cathode potential on H_2O_2 production (a), phenol degradation efficiency (b) and degradation of different pollutants (c), corresponding TOC removal in 120 min for methyl orange and 180 min for phenol and florfenicol (d) by cPANI/GF2.

mainly controlled by the production and activation of H_2O_2, which could be affected by the applied potential as it controls the transfer of electrons between anode and cathode. Therefore, the effect of different cathode potentials on H_2O_2 accumulation and phenol degradation with cPANI/GF2 as the cathode was explored and the results are presented in Fig. 6a and b. The H_2O_2 accumulation increased with the cathode potential increasing from –0.4 V to –0.6 V (vs Ag/AgCl) and then decreased with the potential further increasing to –0.8 V, showing the best performance at –0.6 V (Fig. 6a). These results are in accordance with the literature, where H_2O_2 production first increased with the increase in applied potential until an optimum value is reached and then decreased with further increase in potential [4,36]. This could be explained by the fact that the increase in cathode potential accelerates the transfer of electron, which would result in more reactants convert to the product, however, further increase in potential may result in several side reactions including 4e– ORR [36] (Eq. (3)), hydrogen evolution reaction (Eq. (4)) and/or degradation of H_2O_2 (Eq. (5)) on the cathode surface [52]. The similar trend was also observed for the degradation of

phenol (Fig. 6b). The phenol degradation improved with the increase in applied potential and the maximum value (85%) was obtained at –0.6 V, after which the phenol degradation declined with further increase in potential. It could be attributed to the lower H_2O_2 production at potentials other than –0.6 V that would result in lower concentration of ˙OH generation and thus lesser degradation. The applied potential might affect both the production and activation of H_2O_2 to ˙OH. As shown in Fig. 6a, H_2O_2 production at –0.4 V (43.76 mg/L) was close to –0.6 V (46.14 mg/L), however, the degradation of phenol at –0.4 V (68%) was much lower than that at –0.6 V (85%). This might be due to relatively less activation of H_2O_2 to ˙OH at lower applied potential.

$$2H^+ + 2e^- \rightarrow H_2 \quad (4)$$

$$H_2O_2 + 2H^+ + 2e^- \rightarrow 2H_2O \quad (5)$$

Furthermore, the MO and FLO were used as typical refractory organic pollutants [36,53] to evaluate the consistency of degradation performance for metal-free e-Fenton with cPANI/GF2 as the cathode. For better comparison, initial concentrations of the pollutants were kept at 50 mg/L, same with the concentration of phenol in previous experiments. As shown in Fig. 6c, complete degradation of MO (100%) and FLO (99%) was achieved within 90 min, while degradation of phenol was 85% in 180 min. This slight variation in removal efficiency could be attributed to the stability and chemical structure of the target contaminant. Furthermore, the mineralization efficiency of about 53% for MO and 74% for FLO was achieved as compared to 42% for phenol in 180 min as revealed by the TOC analysis results (Fig. 6d). These results showed that cPANI/GF2 as a cathode in metal-free e-Fenton process could universally degrade refractory organic pollutants.

The pollutants degradation and H_2O_2 production performance of cPANI/GF2 cathode were compared with the literature and found comparable or even better than some reported studies (Table S1). Whereas iron leaching in a homogeneous or even heterogeneous e-Fenton system is inevitable [14], the most significant feature of cPANI/GF2 cathode was its efficient degradation performance without iron catalyst, which would eliminate the secondary metal pollution. Furthermore, as there was no risk of catalyst washout, this cathode could be used in a continuous flow mode, which has reportedly three times higher treatment capacity as compared to the batch system [54].

3.3. Possible catalysis mechanism of the modified electrode

To illustrate the catalysis mechanism of metal-free e-Fenton with cPANI/GF2 as the cathode and evaluate the role of ˙OH, series of experiments were conducted under different controlled conditions and the results are presented in Fig. 7a. It can be seen that simple adsorption and electro sorption (adsorption + electrochemical degradation) of phenol in N_2 saturated solution was much lower than that of metal-free e-Fenton degradation by cPANI/GF2 in the oxygen saturated conditions (Fig. 7a). For instance, there was only 22.92% and 34.85% phenol removal by adsorption and electro sorption as compared to 85.62% in the oxygen saturated conditions, revealing that the adsorbed pollutants could be further degraded by ˙OH during e-Fenton process. To demonstrate the role of free radicals, methanol (20 mL) was added into the electrolyte solution as ˙OH scavenger [18]. As a result, the phenol removal dramatically decreased to only 12% in the absence of ˙OH. As we know that methanol can also prevent the pollutants adsorption, this phenol removal could be ascribed to electrochemical degradation [16]. It is also evident from above results where removal by electro sorption is about 12% higher than the only adsorption. Therefore, it can be said that free hydroxyl radicals were the main oxidants produced from activation of in situ generated H_2O_2 simultaneously catalyzed by cPANI/GF2 cathode. Meanwhile, the production of ˙OH was further confirmed by DMPO spin-trap ESR spectroscopy. As shown in Fig. 7b, the ESR spectra exhibited typical 4 peaks with an intensity ratio of 1:2:2:1, which is a characteristic peak of DMPO/˙OH complex [18,36,55].

In addition, performance of cPANI/GF2 cathode for phenol degradation was compared with the conventional metal-based e-Fenton (EF-Fe) using GF as the cathode and Fe^{+2} (0.2 M) as the catalyst, while all other conditions were kept constant with the previous experiment. As shown in Fig. 7a, EF-Fe showed about 91% phenol degradation, slightly higher (˜6%) than the metal-free e-Fenton degradation. Initially, the cPANI/GF2 cathode showed relatively faster degradation as compared to EF-Fe, which slowed down after 120 min. The corresponding phenol removal rate was also higher than EF-Fe (Fig. S5), which gradually decreased with the passage of time. As there was no dissolved catalyst in the metal-free e-Fenton system, the ˙OH was only generated on the surface of cPANI/GF2 cathode. Therefore, at lower concentrations, limited mass transfer of phenol to the cathode and ˙OH from cathode surface to the bulk solution controlled the degradation process in batch system. Unlike metal-free e-Fenton system, dissolved iron catalyst in EF-Fe could generate ˙OH in the bulk solution and degrade the pollutant independent of the mass transfer to cathode. However, it generates inevitable iron related secondary pollution, thus could not be applied as a sustainable and environmentally friendly treatment solution.

Accordingly, the possible catalysis mechanism of cPANI/GF2 cathode was proposed in Fig. 7c. First, the adsorbed oxygen was converted to H_2O_2 at cathode surface via 2e– ORR process catalyzed by the active sites, which is mainly the graphitic N [20,56]. Then the pyridinic N as an active site could transfer an electron to H_2O_2 to generate ˙OH on the cathode surface [20]. The defects and edges introduced during carbonization might also serve as active sites in the catalysis process [18,48,57]. Some of the generated H_2O_2 was released to the bulk solution that led to its accumulation, which could be activated to ˙OH later by interaction with the cPANI/GF2 cathode surface. Then generated ˙OH both on the cathode and in bulk could attack the organic pollutants, adsorbed to the surface or dissolved in the solution, to degrade them into corresponding by-products. As lifetime (˜20 ns) and diffusion length (˜6 nm) of ˙OH is very short [11], existence of pollutants and oxidants in close proximity would increase ˙OH utilization and enhance the degradation.

3.4. Stability of the modified electrode

Stability of the cPANI/GF2 cathode was studied by conducting series of H_2O_2 production experiments for 5 cycles (C1–C5) using the same electrode without any treatment between successive cycles. The results revealed that cPANI/GF2 could stably produce H_2O_2 for 5 consecutive cycles (Fig. 8a). Furthermore, cPANI/GF2 was also tested for degradation of organic pollutants for 3 consecutive cycles. The results revealed that reusability of the electrode could vary for different pollutants (Fig. 8b). The phenol removal efficiency decreased to about 42% in C2 and C3. These results are consistent with the reported literature where the phenol removal efficiency was 50% of the fresh electrode in the second cycle [34], while better than that only 20% phenol removal reported in the second cycle [18]. However, the degradation efficiency of MO remained above 99% for all the 3 cycles (every experiment for MO degradation lasts for 120 min). For FLO, the degradation was about 90% and 62% for C2 and C3. As previously explained, this might be ascribed to the blockage of the active sites, which were responsible for the activation of H_2O_2 to generate ˙OH by the degradation by-products [18]. Some similar studies about metal-free e-Fenton suggested that the actives sites of the used cathode could be easily recovered by simply rinsing the electrode with ethanol or clean water [18–20]. The varying reusability performance of the electrode for MO and FLO could be due to different kinds of degradation by-products and their adsorption behavior to the active sites. Furthermore, stability of the coated nanofibers network was confirmed by the SEM analysis of the used electrode, which showed no obvious change in the surface morphology after 5 cycles (Fig. S6). These results confirmed that cPANI/GF2 could be used as a cathode to degrade refractory organic pollutants in a metal-free e-

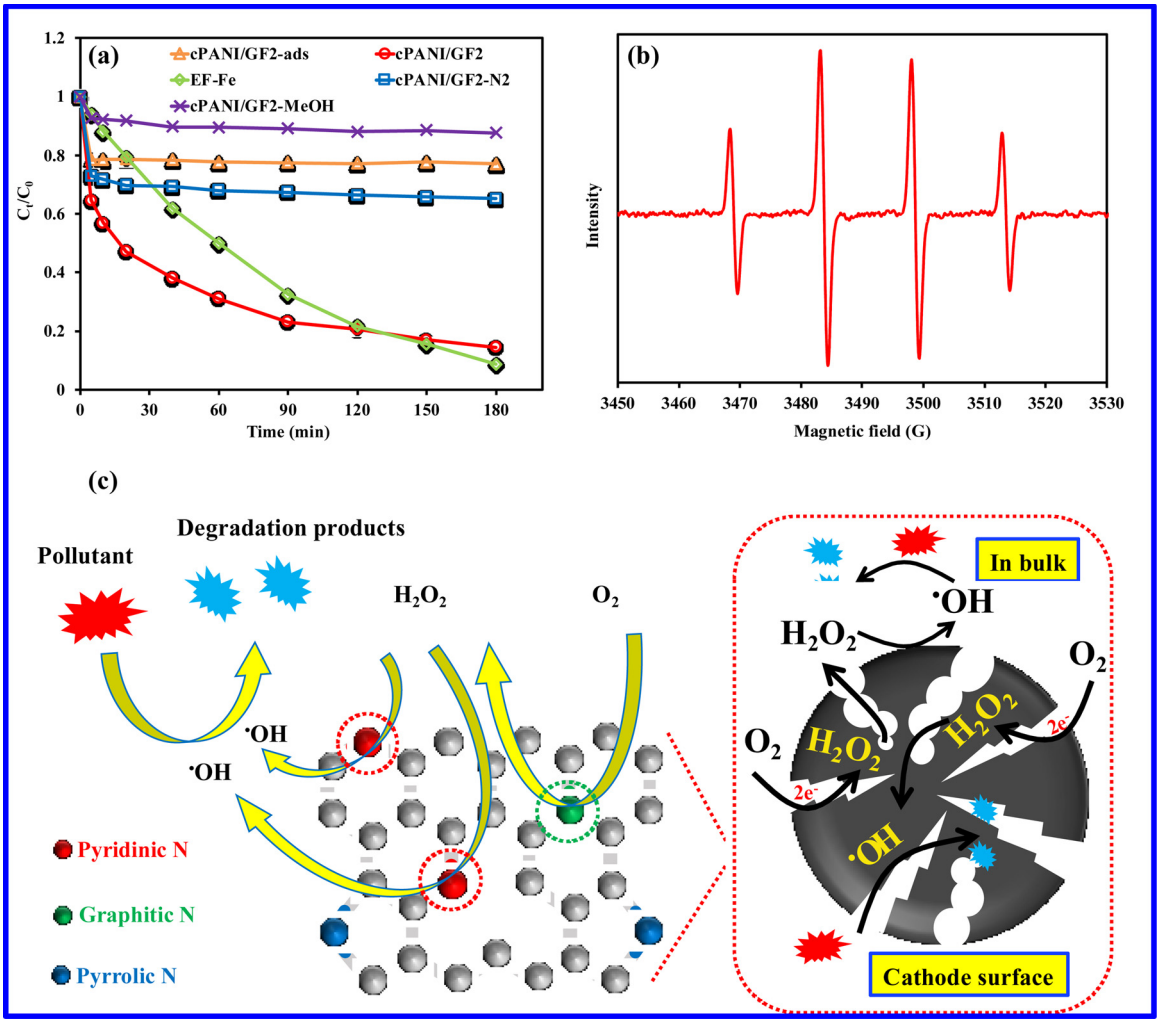

Fig. 7. The phenol degradation at different conditions, and the comparison with conventional iron based EF process (a); ESR spectrum of ˙OH using DMPO trapping agent (b) and possible catalysis mechanism (c) of cPANI/GF2 in a metal-free e-Fenton system. Conditions: V 100 mL, methanol 20 mL, 0.05 M Na_2SO_4 at pH 3, C_0 50 mg/L, potential -0.6 V v Ag/AgCl, Fe^{+2} 0.2 mM.

Fenton system. Furthermore, the active material loaded by in situ fabrication process without any binder could remain stable for long-term operation.

4. Conclusions

In this study, a graphite felt electrode was in situ modified using PANI derived N-doped carbon nanofibers without any binder and used in the metal-free e-Fenton process as a novel cathode for refractory

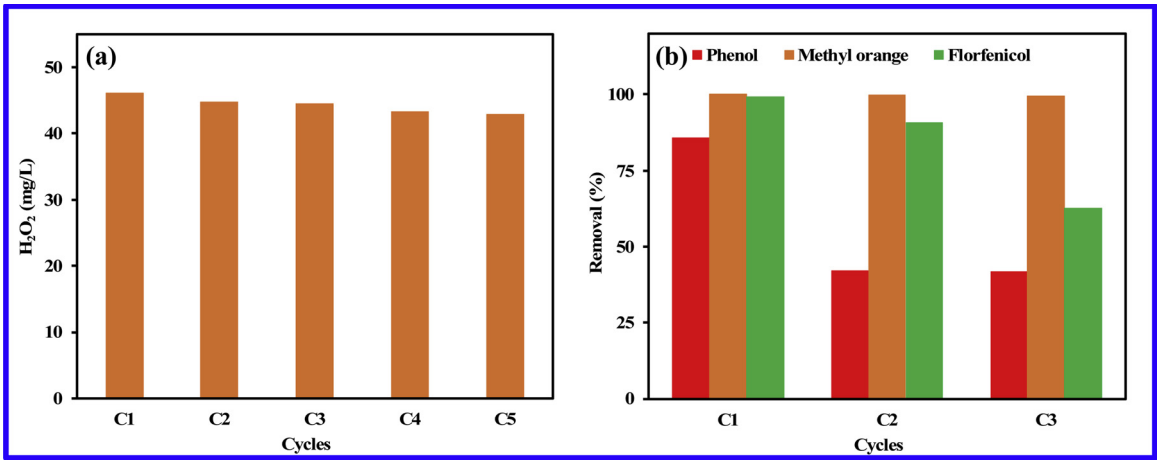

Fig. 8. Stability of cPANI/GF2 as a metal-free e-Fenton cathode for H_2O_2 production (a) and degradation of organic pollutants (b).

organics degradation in wastewater. The prepared cPANI/GF2 electrode was very stable without any binders, which could reduce the extra cost and intricate electrode fabrication process. The KOH activation tailored the surface functional groups, which significantly enhanced the catalytic performance of the electrode. The etching by KOH reduced the overall nitrogen content but there was a trade-off between different nitrogen functional groups and specific surface area, which can be controlled by simply varying the KOH concentration. The optimized cPANI/GF2 electrode showed satisfactory degradation performance for phenol (85%), florfenicol (99%) and methyl orange (100%). Furthermore, from an application point of view, the cPANI/GF2 could be a potential sustainable cathode for in situ generation of H_2O_2 and $^{\cdot}OH$ for the degradation of variety of organic contaminants without any externally added chemicals, as compared to the iron-based e-Fenton, which inevitably generate metal sludge as secondary pollutant.

Acknowledgment

This research was financially supported by National Natural Science Foundation of China (No. 21577162), the Interdisciplinary Innovation Team Program of the Chinese Academy of Sciences (No. 2015, Team of directional biotransformation of environmental pollutants) and the CAS Key Laboratory of Environmental Biotechnology. Muhammad Rizwan Haider acknowledges the CAS-TWAS President's Fellowship for International PhD Students.

Appendix A. Supplementary data

Supplementary material related to this article can be found, in the online version, at doi:https://doi.org/10.1016/j.apcatb.2019.117774.

References

[1] F. Yu, M. Zhou, X. Yu, Electrochim. Acta 163 (2015) 182–189.
[2] L. Zhou, M. Zhou, Z. Hu, Z. Bi, K.G. Serrano, Electrochim. Acta 140 (2014) 376–383.
[3] E. Brillas, I. Sirés, M.A. Oturan, Chem. Rev. 109 (2009) 6570–6631.
[4] Y. Wang, Y. Liu, K. Wang, S. Song, P. Tsiakaras, H. Liu, Appl. Catal. B 165 (2015) 360–368.
[5] S. Yuan, Y. Fan, Y. Zhang, M. Tong, P. Liao, Environ. Sci. Technol. 45 (2011) 8514–8520.
[6] M. Pimentel, N. Oturan, M. Dezotti, M.A. Oturan, Appl. Catal. B 83 (2008) 140–149.
[7] Z. Pan, K. Wang, Y. Wang, P. Tsiakaras, S. Song, Appl. Catal. B 237 (2018) 392–400.
[8] X. Zhang, J. Fu, Y. Zhang, L. Lei, Sep. Purif. Technol. 64 (2008) 116–123.
[9] W. Yang, M. Zhou, J. Cai, L. Liang, G. Ren, L. Jiang, J. Mater. Chem. A 5 (2017) 8070–8080.
[10] T.X.H. Le, M. Bechelany, S. Lacour, N. Oturan, M.A. Oturan, M. Cretin, Carbon 94 (2015) 1003–1011.
[11] W. Zhou, L. Rajic, L. Chen, K. Kou, Y. Ding, X. Meng, Y. Wang, B. Mulaw, J. Gao, Y. Qin, A.N. Alshawabkeh, Electrochim. Acta 296 (2018) 317–326.
[12] X. Qian, M. Ren, Y. Zhu, D. Yue, Y. Han, J. Jia, Y. Zhao, Environ. Sci. Technol. 51 (2017) 3993–4000.
[13] N. Barhoumi, H. Olvera-Vargas, N. Oturan, D. Huguenot, A. Gadri, S. Ammar, E. Brillas, M.A. Oturan, Appl. Catal. B 209 (2017) 637–647.
[14] M. Hartmann, S. Kullmann, H. Keller, J. Mater. Chem. 20 (2010) 9002–9017.
[15] D. Yue, X. Qian, M. Kan, M. Fang, J. Jia, X. Yang, Y. Zhao, Appl. Catal. B 229 (2018) 211–217.
[16] H. Luo, C. Li, C. Wu, W. Zheng, X. Dong, Electrochim. Acta 186 (2015) 486–493.
[17] H. Dong, H. Su, Z. Chen, H. Yu, H. Yu, Electrochim. Acta 222 (2016) 1501–1509.
[18] W. Yang, M. Zhou, L. Liang, Chem. Eng. J. 338 (2018) 700–708.
[19] W. Yang, M. Zhou, N. Oturan, Y. Li, P. Su, M.A. Oturan, Electrochim. Acta 297 (2019) 582–592.
[20] P. Su, M. Zhou, X. Lu, W. Yang, G. Ren, J. Cai, Appl. Catal. B 245 (2019) 583–595.
[21] R. Sha, S. Badhulika, Electrochim. Acta 251 (2017) 505–512.
[22] G. Divyapriya, P. Thangadurai, I. Nambi, ACS Sustainable Chem. Eng. 6 (2018) 3453–3462.
[23] J. Luo, V.C. Tung, A.R. Koltonow, H.D. Jang, J. Huang, J. Mater. Chem. 22 (2012) 12993–12996.
[24] T. Zhu, J. Zhou, Z. Li, S. Li, W. Si, S. Zhuo, J. Mater. Chem. A 2 (2014) 12545–12551.
[25] N.A. Khan, H.J. An, D.K. Yoo, S.H. Jhung, J. Hazard. Mater. 360 (2018) 163–171.
[26] Z. Zhao, Y. Xie, L. Lu, Electrochim. Acta 283 (2018) 1618–1631.
[27] C. Xiong, T. Li, Y. Zhu, T. Zhao, A. Dang, H. Li, X. Ji, Y. Shang, M. Khan, J. Alloys Compd. 695 (2017) 1248–1259.
[28] Y. He, X. Wang, H. Huang, P. Zhang, B. Chen, Z. Guo, Appl. Surf. Sci. 469 (2019) 446–455.
[29] G. Wu, K.L. More, C.M. Johnston, P. Zelenay, Science 332 (2011) 443.
[30] D. Guo, R. Shibuya, C. Akiba, S. Saji, T. Kondo, J. Nakamura, Science 351 (2016) 361–365.
[31] D.K. Yoo, H.J. An, N.A. Khan, G.T. Hwang, S.H. Jhung, Chem. Eng. J. 352 (2018) 71–78.
[32] R. Silva, D. Voiry, M. Chhowalla, T. Asefa, J. Am. Chem. Soc. 135 (2013) 7823–7826.
[33] R.M. Sellers, Analyst 105 (1980) 950–954.
[34] E. Saputra, S. Muhammad, H. Sun, S. Wang, RSC Adv. 3 (2013) 21905–21910.
[35] L.H. Yang, T.T. Zhu, W.W. Cai, M.R. Haider, H.C. Wang, H.Y. Cheng, A.J. Wang, Bioresour. Technol. 268 (2018) 176–182.
[36] W.L. Jiang, X. Xia, J.L. Han, Y.C. Ding, M.R. Haider, A.J. Wang, Environ. Sci. Technol. 52 (2018) 9972–9982.
[37] X. Li, Z.Y. Sui, Y.N. Sun, P.W. Xiao, X.Y. Wang, B.H. Han, Microporous Mesoporous Mater. 257 (2018) 85–91.
[38] Z. Mo, H. Peng, H. Liang, S. Liao, Electrochim. Acta 99 (2013) 30–37.
[39] Z. Tong, Y. Yang, J. Wang, J. Zhao, B.-L. Su, Y. Li, J. Mater. Chem. A 2 (2014) 4642–4651.
[40] H. Zhang, Q. Zhao, S. Zhou, N. Liu, X. Wang, J. Li, F. Wang, J. Power Sources 196 (2011) 10484–10489.
[41] B. Lu, T.J. Smart, D. Qin, J.E. Lu, N. Wang, L. Chen, Y. Peng, Y. Ping, S. Chen, Chem. Mater. 29 (2017) 5617–5628.
[42] S. Jiang, Z. Li, H. Wang, Y. Wang, L. Meng, S. Song, Nanoscale 6 (2014) 14262–14269.
[43] J. Zhang, Z. Xia, L. Dai, Science Advances 1 (2015) e1500564.
[44] Z. Zhang, Z. Zhou, H. Peng, Y. Qin, G. Li, Electrochim. Acta 134 (2014) 471–477.
[45] R.L. Zornitta, F.J. García-Mateos, J.J. Lado, J. Rodríguez-Mirasol, T. Cordero, P. Hammer, L.A.M. Ruotolo, Carbon 123 (2017) 318–333.
[46] J.R. Pels, F. Kapteijn, J.A. Moulijn, Q. Zhu, K.M. Thomas, Carbon 33 (1995) 1641–1653.
[47] J. Liu, Y. Qiao, C.X. Guo, S. Lim, H. Song, C.M. Li, Bioresour. Technol. 114 (2012) 275–280.
[48] P. Hu, H. Su, Z. Chen, C. Yu, Q. Li, B. Zhou, P.J.J. Alvarez, M. Long, Environ. Sci. Technol. 51 (2017) 11288–11296.
[49] H. Miao, S. Li, Z. Wang, S. Sun, M. Kuang, Z. Liu, J. Yuan, Int. J. Hydrogen Energy 42 (2017) 28298–28308.
[50] J. Yu, T. Liu, H. Liu, Y. Wang, Chin. J. Catal. 37 (2016) 2079–2085.
[51] G. Wu, Z.W. Chen, K. Artyushkova, F.H. Garzon, P. Zelenay, Proton Exchange Membrane Fuel Cells 8, Pts 1 and 2, Electrochemical Soc Inc, Pennington, 2008 159.
[52] D. Li, T. Sun, L. Wang, N. Wang, Electrochim. Acta 282 (2018) 416–426.
[53] Y. Xiao, J.M. Hill, Environ. Sci. Technol. 52 (2018) 11760–11768.
[54] I. De la Obra Jiménez, B. Esteban García, G. Rivas Ibáñez, J.L. Casas López, J.A. Sánchez Pérez, Appl. Catal. B 247 (2019) 115–123.
[55] H. Zhao, L. Qian, X. Guan, D. Wu, G. Zhao, Environ. Sci. Technol. 50 (2016) 5225–5233.
[56] J. Liu, P. Song, M. Ruan, W. Xu, Chin. J. Catal. 37 (2016) 1119–1126.
[57] X. Duan, H. Sun, Z. Ao, L. Zhou, G. Wang, S. Wang, Carbon 107 (2016) 371–378.